Article

Analysis of Singlet Oxygen Luminescence Generated By Protoporphyrin IX

Vikas Vikas [1],*, Weibing Yang [2], Brian C. Wilson [3], Timothy C. Zhu [2] and Robert H. Hadfield [1],*

[1] Electronic & Nanoscale Engineering, James Watt School of Engineering, University of Glasgow, Glasgow G128QQ, UK
[2] Department of Radiation Oncology, University of Pennsylvania, Philadelphia, PA 19104, USA; weibing.yang@pennmedicine.upenn.edu (W.Y.); timothy.zhu@pennmedicine.upenn.edu (T.C.Z.)
[3] Department of Medical Biophysics, University Health Network/University of Toronto, Toronto, ON M5G 2C4, Canada; brian.wilson@uhn.ca
* Correspondence: vikas.vikas.2@glasgow.ac.uk (V.V.); robert.hadfield@glasgow.ac.uk (R.H.H.)

Abstract: The effectiveness of photodynamic therapy (PDT) for cancer treatment relies on the generation of cytotoxic singlet oxygen ($^1O_2$) in type II PDT. Hence, monitoring of $^1O_2$ generation during PDT enables optimal treatment delivery to the tumor target with reduced off-target effects. Direct $^1O_2$ observation by measuring its luminescence at 1270 nm remains challenging due to the very weak signal. This study presents $^1O_2$ luminescence measurements using a time-resolved singlet oxygen luminescence detection system (TSOLD) applied to protoporphyrin IX (PpIX) in different solvents (ethanol and acetone) and biological media (bovine serum albumin and agarose-based solid phantom). The compact experimental setup includes a nanosecond diode laser with a function generator, a cuvette with photosensitizer solution, optical filtering and mirrors, an InGaAs single-photon avalanche diode detector, and time-tagger electronics. Increasing the concentration of PpIX in these media from 1 to 10 μg/g resulted in a 3–5 × increase in the $^1O_2$ luminescence signal. Furthermore, increasing light scattering in the sample using Intralipid from 0.1 to 1% led to a decrease in the $^1O_2$ luminescence signal and lifetime. These results confirm the marked effect of the microenvironment on the $^1O_2$ signal and, hence, on the photodynamic efficacy.

Keywords: reactive oxygen species; singlet oxygen; photodynamic therapy; protoporphyrin IX; time-resolved singlet oxygen luminescence detection

1. Introduction

Photodynamic therapy (PDT) is a minimally invasive therapeutic modality that has been used for a variety of malignant and non-malignant conditions [1–3]. PDT for cancer treatment utilizes light, a photosensitizer (PS) and molecular oxygen to induce localized cell death by multiple mechanisms such as cell death by immune response [3–5]. In the so-called Type I pathway, the photoexcited triplet-state photosensitizer interacts with cellular substrates, most commonly membranes, to produce free radicals and reactive oxygen species (ROS) such as superoxide, hydroxyl radicals and hydrogen peroxide [6,7]. As shown in Figure 1, in the Type II pathway that pertains to most clinical photosensitizers, the excited triplet-state PS transfers energy to triplet ground-state molecular oxygen ($^3O_2$), generating highly reactive singlet oxygen ($^1O_2$) [8–10]. Hence, sensitive monitoring of $^1O_2$ during PDT should enable optimal treatment delivery to the tumor target with reduced off-target effects [3]. A variety of approaches have been investigated for PDT dosimetry, including

biophysical/biological tissue response monitoring, explicit dosimetry in which the light, photosensitizer and tissue oxygenation are measured and combined into a biophysical model, and implicit dosimetry in which a surrogate measure such as photosensitizer photobleaching is used [4,10,11].
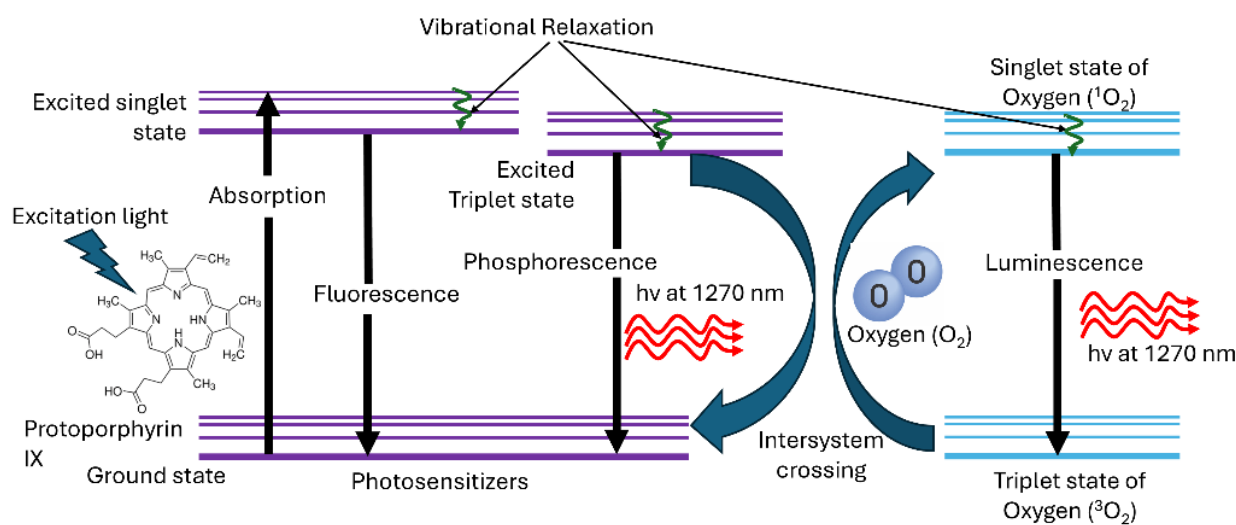

Figure 1. Jablonski diagram illustrating the generation of the 1270 nm near-infrared luminescence emission of singlet oxygen ($^1O_2$) and triplet-state photosensitizer luminescence.

The direct technique of singlet oxygen luminescence dosimetry (SOLD) uses observation of the 1270 nm near-infrared luminescence emission of the $^1O_2 \rightarrow {}^3O_2$ transition [12–14]. Since this directly quantifies the concentration of cytotoxic species, it can be considered the "gold standard" for PDT dosimetry. However, measurement is challenging due to the very low signal and the short half-life in biological media. Detection is significantly improved by the use of single-photon counting using NIR photomultiplier tubes (PMTs), InGaAs single-photon avalanche diodes (SPADs) and superconducting nanowire single-photon detectors (SNSPDs) [15–18]. Time-resolved single-photon counting (TSOLD) and gating allow for the subtraction of the contribution of the substantial background due to photosensitizer fluorescence and phosphorescence [13,17,19–21], while fitting the temporal spectrum yields the singlet oxygen and PS triplet-state lifetimes. Typically, measurements are made on and at wavelengths either side of the 1270 nm peak to subtract the residual background after long-pass filtering of the total emission. TSOLD has been validated through multiple in vitro and in vivo studies in cells, tumors and normal tissues [13,22].

TSOLD can be implemented using commercially available SPADs and SNSPDs with low dark count rates, low timing jitter and free-running operation. Here, we developed a versatile TSOLD testbed that incorporates a nanosecond diode excitation laser with a function generator that provides external triggering to select a suitable repetition rate, a cuvette containing the photosensitizer solution, custom optical filtering and mirrors, an InGaAs SPAD detector and time-resolved electronics.

The choice of photosensitizer plays a critical role in the efficacy and specificity of PDT treatments. An ideal photosensitizer should possess a high $^1O_2$ quantum yield, strong absorption in the therapeutic window (~600–800 nm) and selective accumulation in the target cells/tissues [2,23]. Porphyrin-based compounds, such as porfimer sodium (Photofrin®), and protoporphyrin IX (PpIX) synthesized in target cells by administration of aminolevulinic acid, were among the first photosensitizers approved for clinical use [24,25]. However, there is a gap in knowledge of the lifetime and efficacy of $^1O_2$ produced by PpIX photoactivation in various microenvironments [26]. Here, we performed a comprehensive study utilizing our in-house TSOLD system with PpIX in ethanol, acetone, bovine serum

albumin (BSA) and agarose-based solid phantoms. The impact of light scattering on the $^1O_2$ generation was determined by adding the lipoprotein Intralipid with either ethanol or methanol solvents to mimic a tissue-like microenvironment. This study of $^1O_2$ luminescence detection by PpIX in various solvents and biological media is the first set towards future applications such as dosimetry for PDT.

2. Materials and Methods

2.1. Time-Resolved $^1O_2$ Luminescence System

The system (Figure 2) is designed to measure the near-infrared singlet oxygen luminescence that comprises a nanosecond diode excitation laser with a function generator, a quartz cuvette (CV10Q35, Thorlabs, Newton, NJ, USA) containing photosensitizer solution, customized optical filtering and mirrors, a single-photon avalanche diode (SPAD) detector, and time-tagger electronics for time-correlated single-photon counting (TCSPC).
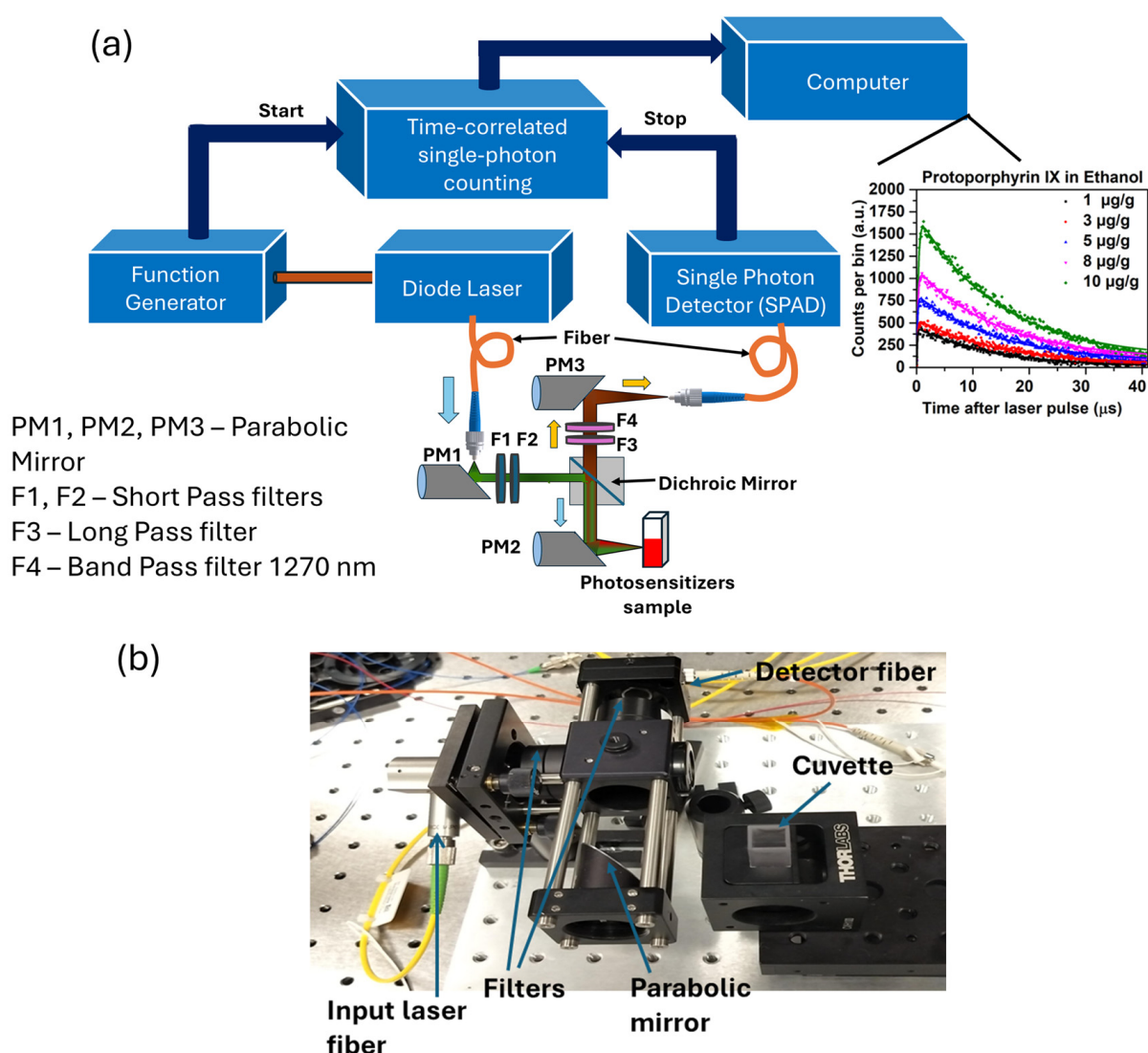

Figure 2. (**a**) Schematic and optical setup of the TSOLD experiment (upper). An optical beam from a nanosecond diode laser with a function generator illuminates the photosensitizer cuvette through a parabolic mirror and short-pass filters. The collected 1270 nm luminescence emission is coupled into an InGaAs-SPAD. TCSPC then generates time histograms of the $^1O_2$ luminescence signal. (**b**) A photograph of the optical setup is shown (lower).

The 6–129 ns pulse-width tunable diode laser (NPL52C: Thorlabs, Newton, NJ, USA) has a broad spectral output of 515–525 nm and a variable repetition rate up to 50 kHz. The wavelength of the illuminated laser (520 nm) was selected corresponding to the secondary absorption region of PpIX. The output is coupled into a multimode optical fiber (core diameter 400 μm, 0.22 numerical aperture (M146L01, Thorlabs, Newton, NJ, USA)) connected to a collimation system consisting of a parabolic mirror (RC04FC-P01, Thorlabs, Newton, NJ, USA) and 25 mm diameter short-pass (optical density OD = 5.0 at >950 nm) (FESH0950, Thorlabs, Newton, NJ, USA) and band-pass (304–785 nm: out-of-band OD = 4.0) (FGS550, Thorlabs, Newton, NJ, USA) filters to produce a 4 mm collimated beam that is reflected by a dichroic mirror (DMLP950, Thorlabs, Newton, NJ, USA) and focused into the cuvette using a parabolic mirror to illuminate the sample. The 1270 nm luminescence emission passes through a dichroic mirror and the combination of long-pass (OD = 5.0 at <1200 nm: FELH1200, Thorlabs) and band-pass filters (bandwidth 1260–1280 nm, out-of-band OD = 6.0) (1270BP20, Omega Optical, Brattleboro, VT, USA). The beam is then coupled to a multimodal, 65 μm core diameter fiber to the SPAD detector (ID230, IDQ, Geneva, Switzerland) using a parabolic mirror. The TCSPC module (Time Tagger Ultra, Swabian Instruments, Stuttgart, Germany) counts the input signals from the function generator, sending a START signal through an electrical synchronization pulse, and the detector output then provides the STOP signal. Temporal histograms are thereby generated from single-photon detection events. Pulse pile-up can cause errors in the determination of the $^1O_2$ lifetime so that the detection count rate is kept below 5% of the excitation laser pulse rate.

2.2. Photosensitizer in Various Media

The photosensitizer solutions were prepared by dissolving protoporphyrin IX (PpIX) (P8293, Sigma Aldrich, St. Louis, MO, USA) powder in ethanol or acetone. The molecular weight of PpIX is 562.66 g/mol and its molecular structure is shown in Figure 3. For the bovine serum albumin (BSA) and solid phantoms, the PpIX was dissolved first in dimethyl sulfoxide (DMSO). A 50 μg/g BSA solution was prepared by dissolving BSA powder (A9647, Sigma Aldrich) in phosphate-buffered saline (PBS). The solid phantoms were prepared using 1% agarose (A9539, Sigma Aldrich, St. Louis, MO, USA) dissolved in deionized water as the base material [27], mixed with the PpIX-DMSO solution and maintained at room temperature (20–25 °C) to solidify. For each TSOLD experiment, the PpIX was used at 1, 3, 5, 8 and 10 μg/g concentrations in 1 mL samples.
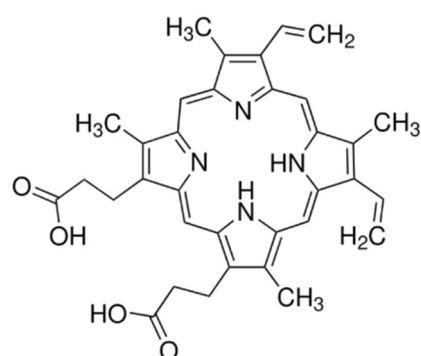

Figure 3. Molecular structure of PpIX [28].

2.3. Determination of Singlet Oxygen Lifetime

Singlet oxygen generation occurs due to energy transfer from a triplet-state photosensitizer exchanging energy with triplet ground-state oxygen ($^3O_2$). For short pulse activation

($\leq$100 ns), the lifetime of singlet oxygen and triplet-state photosensitizers at time *t* following the pulse is given by Refs. [12,29]:

$$[1_{O_2}](t) = N\sigma[S_0]\varphi_D \cdot \frac{\tau_D}{\tau_T - \tau_D}\left(\exp\left(\frac{-t}{\tau_T}\right) - \exp\left(\frac{-t}{\tau_D}\right)\right) \tag{1}$$

where $[^1O_2]$ (*t*) is the singlet oxygen concentration, N is the number of photons per pulse, σ is the photosensitizer absorption cross-section at the excitation wavelength, $[S_0]$ is the photosensitizer concentration, φ_D is the photosensitizer singlet oxygen quantum yield, and τ_D and τ_T are the lifetimes of the singlet oxygen and triplet-state photosensitizer, respectively. After subtracting the background signal due to other sources of near-infrared emission, the measured time histograms were fitted using Equation (1) to calculate the two lifetimes.

2.4. Validation of TSOLD System

Before measuring the $^1O_2$ luminescence signature from PpIX in different microenvironments, the TSOLD system performance was validated against measurements made with a set of 20 nm bandwidth band-pass filters centered at 1200, 1240, 1270, 1300 and 1340 nm. A solution of 10 μg/g PpIX in ethanol was illuminated by the 520 nm laser beam (520 nm $\pm$ 7.5 nm, 129 ns at 25 kHz) with a beam waist of 0.2 mm and an average intensity of 32 mW.mm^{-2}. Signal acquisition was conducted with the SPAD, operating with 10% single-photon detection efficiency and a 41 μs dead time.

2.5. $^1O_2$ Luminescence from PpIX in Ethanol and Acetone

Measurements were made using 10 min signal integration with 1–10 μg/g PpIX solution in 1 mL cuvettes with a path length of 10 mm, using a 1 mm diameter beam at 520 nm $\pm$ 7.5 nm, at 20 or 3.2 mW.mm^{-2} in ethanol and acetone, respectively. The SPAD was operated at 10% efficiency with 41 μs dead time to avoid pulse pile-up. Histograms were generated with 610 bins with a 65 ns width. These were fitted using Equation 1 using the Levenberg–Marquardt algorithm.

2.6. $^1O_2$ Luminescence from PpIX in Biological Media

Measurement of singlet oxygen generation in cells and tissues is of value for dosimetry in photodynamic therapy. BSA and tissue-mimicking phantoms were excited by a 2 mm diameter laser beam at 5.5 mW.mm^{-2}, 129 ns pulse width and 30 kHz repetition rate. The luminescence was measured after passing through a 1270 nm, 20 nm bandwidth filter using a SPAD with 25% efficiency and 34 μs dead time. Time histograms of 520 bins with a bin width of 65 ns were generated by capturing single-photon arrival events using the Time Tagger. These plots were fitted with Equation 1, used to calculate the $^1O_2$ and photosensitizer triplet-state lifetimes.

2.7. Impact of Scattering on Singlet Oxygen Generation and Luminescence Lifetime

The scattering properties of a sample can affect the production of singlet oxygen [30] due to altered light fluence in the sample. Intralipid emulsion is commonly used as a light-scattering medium [31]. Here, 20% Intralipid (I141, Sigma Aldrich, St. Louis, MO, USA) diluted to 0.1–1% (after accounting for the 20% concentration of the stock commercial material) was added to a solution of 10 μg/g PpIX in 100% pure ethanol or acetone.

3. Results and Discussion

Figure 4 shows the results of measuring the singlet oxygen luminescence of 10 μg/g PpIX in ethanol using the multiple band-pass filters.
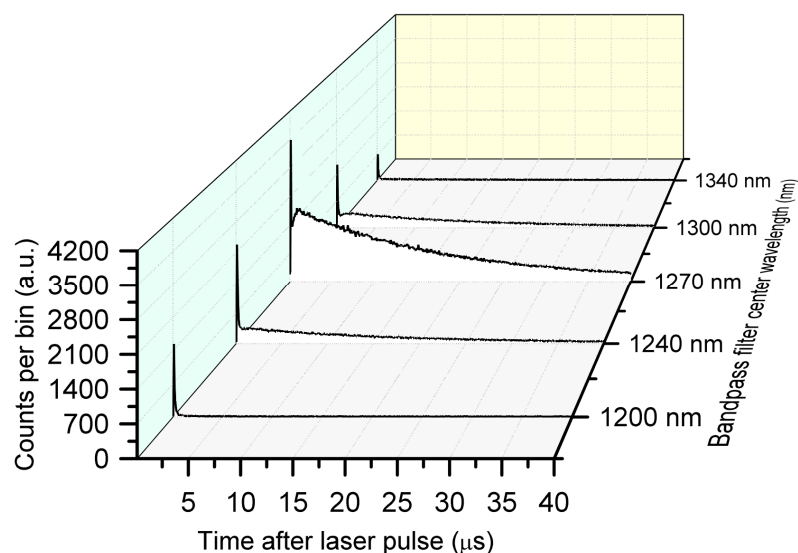
Figure 4. TCSPC histograms for 10 μg/g PpIX in ethanol with 10 min acquisition time using discrete band-pass filters showing the 1270 nm $^1O_2$ luminescence peak and signal decay.

Figure 5 shows the 1270 nm luminescence over time data for PpIX at different concentrations in ethanol and acetone. The derived $^1O_2$ and photosensitizer triplet-state lifetimes are summarized in Table 1.
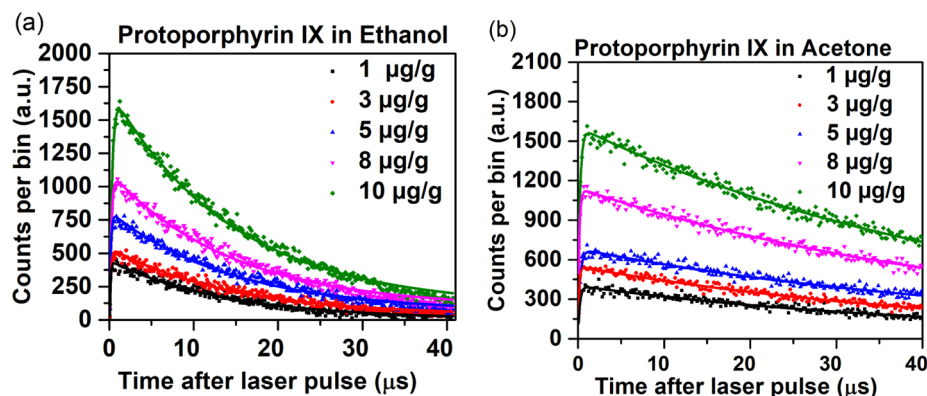

Figure 5. TSOLD single-photon counting time curves (measured dots, fitted lines) at 1270 nm for 1–10 μg/g PpIX in (**a**) ethanol and (**b**) acetone. 10 min integration.

Table 1. Singlet oxygen and photosensitizer triplet-state PpIX lifetimes in ethanol and acetone.

PpIX Concentration (μg/g)	PpIX in Ethanol		PpIX in Acetone	
	Singlet Oxygen Lifetime (μs)	PpIX Triplet-State Lifetime (μs)	Singlet Oxygen Lifetime (μs)	PpIX Triplet-State Lifetime (μs)
1	13.8	0.10	47.9	0.16
3	14.4	0.13	48.2	0.21
5	14.6	0.14	48.3	0.27
8	14.4	0.18	48.4	0.17
10	14.6	0.22	48.6	0.25

As expected, increasing the PpIX concentration had a minimal effect on the $^1O_2$ lifetime in both solvents, but markedly increased the triplet-state lifetimes. The concentration-dependent triplet-state lifetime trend is consistent with previously reported data by Gemmell et al. [19] and is due to the high dose of PpIX.

The corresponding time histograms for PpIX in BSA and the solid phantom with different mass concentrations are shown in Figure 6.
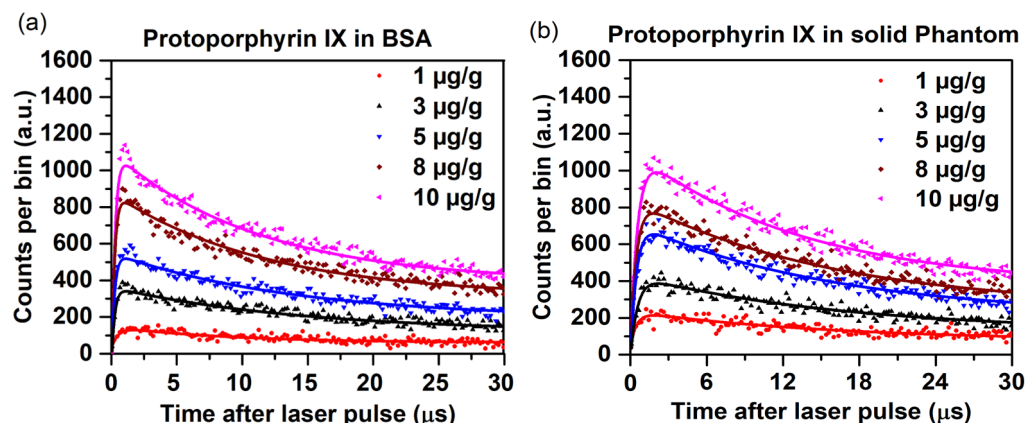

Figure 6. TSOLD single-photon counting time curves (measured dots, fitted lines) at 1270 for 1–10 μg/g PpIX at different concentrations in (**a**) BSA and (**b**) solid agarose. 15 min integration time.

From Figure 6, it is evident that the optimized SPAD efficiency and setup allow time-resolved detection of PpIX in biological-type media, despite the very weak signal. The total time-integrated counts increased 5–6-fold as the PpIX concentration increased from 1 to 10 μg/g. The corresponding $^1O_2$ and triplet-state lifetimes are shown in Table 2.

Table 2. Singlet oxygen and photosensitizer triplet-state PpIX lifetimes in BSA and solid agarose, as per Table 1.

PpIX Concentration (μg/g)	PpIX in BSA		PpIX in Agarose-Based Solid Phantoms	
	Singlet Oxygen Lifetime (μs)	PpIX Triplet-State Lifetime (μs)	Singlet Oxygen Lifetime (μs)	PpIX Triplet-State Lifetime (μs)
1	18.9	0.51	21.1	0.54
3	23.0	0.20	25.4	0.44
5	26.9	0.19	27.5	0.38
8	28.4	0.17	28.8	0.36
10	28.5	0.16	28.9	0.34

The concentration of PpIX in agarose solid phantom directly impacts the $^1O_2$ and triplet-state lifetimes. As the concentration of PpIX increases, excitonic interactions resulting from PPIX stacking and self-absorption become more pronounced, which causes a reduced triplet-state lifetime due to increased quenching and energy dissipation among closely packed PpIX molecules [32–34]. Meanwhile, the $^1O_2$ lifetime increases with concentration in both BSA and agarose due to more efficient energy transfer to oxygen and potentially reduced non-radiative decay in the denser PpIX environment [35]. The photophysical properties and hydrophobicity of the surrounding medium are influenced by the specific interactions of PpIX with its microenvironment, such as protein binding in BSA or the gel matrix in agarose phantoms [36]. These effects are absent in the non-biological solvents. Also, the increase in viscosity of agar can impede the diffusion of singlet oxygen, consequently impacting its longevity and transport mechanisms. The reported studies showed that an increase in viscosity results in a decreased diffusion coefficient for singlet oxygen, thereby reducing diffusion distances and modifying its reactivity [37].

The time curves and fits by using Equation 1 for 10 μg/g PpIX in ethanol and acetone with different concentrations of added Intralipid are shown in Figure 7. The $^1O_2$ luminescence counts decreased with increasing Intralipid concentration by ~5-fold and ~1.5-fold

in ethanol and acetone, respectively. Qualitatively, this can be attributed to the increased scattering of the medium the excitation, and collected light reduces $^1O_2$ luminescence detection [17,38]. The corresponding $^1O_2$ and PpIX triplet-state lifetimes are shown in Table 3.
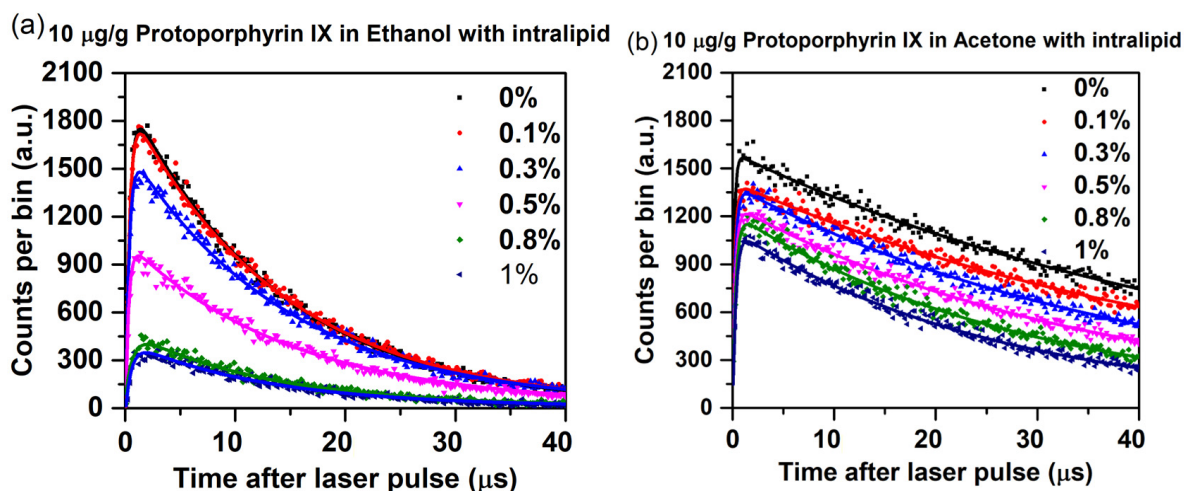

Figure 7. Measured and fitted luminescence plots for 10 μg/g PpIX in (**a**) ethanol and (**b**) acetone at Intralipid concentrations up to 1% using a 10 min acquisition time.

Table 3. Singlet oxygen and PpIX triplet-state lifetimes for 10 μg/g PpIX in ethanol and acetone with varying Intralipid concentration.

Intralipid Concentration (%)	PpIX in Ethanol		PpIX in Acetone	
	Singlet Oxygen Lifetime (μs)	PpIX Triplet-State Lifetime (μs)	Singlet Oxygen Lifetime (μs)	PpIX Triplet-State Lifetime (μs)
0	14.6	0.30	48.6	0.18
0.1	14.4	0.32	48.0	0.24
0.3	14.2	0.34	45.9	0.25
0.5	13.8	0.36	42.1	0.28
0.8	13.3	0.51	40.4	0.31
1.0	12.7	0.55	38.7	0.33

The addition of Intralipid has only a minor impact on the lifetime of singlet oxygen, except for some concentration-dependent reduction with acetone. Also, the PpIX binding to lipoproteins can alter the lifetime of singlet oxygen, which may occur due to the quenching of singlet oxygen by lipoprotein [39,40]. The PpIX triplet-state lifetime is significantly higher in ethanol in the presence of Intralipid and increases markedly with Intralipid concentration, while this effect is much less pronounced with acetone. Increased scattering can result in a prolonged residence time of the triplet state in the excited state, leading to diminished energy transfer efficiency and an extension of the triplet lifetime [41]. Due to different solubility properties of Intralipid in ethanol and acetone, variations in triplet-state lifetime are observed [42]. The residence time of the triplet state in the excited state can range from 100 ns to 10 s, contingent upon intrinsic factors, such as molecular photophysics, as well as extrinsic factors including environmental conditions and quenching agents [43]. Although the scattering properties of the solution do not exert a direct influence on the lifetime, they may affect measurements indirectly by altering signal detection within the scattering medium. Furthermore, variations in oxygen concentration can have a pronounced effect on triplet decay, as this can lead to quenching of the triplet state of protoporphyrin IX (PPIX), resulting in a reduced lifetime through chemical or collisional interactions.

The illumination laser diode (520 nm) wavelength was selected corresponding to the secondary absorption region of PpIX, which allows more effective excitation as well as minimizing background autofluorescence as compared to blue light. Also, the corresponding absorption coefficients of PpIX are higher at 520 nm than red wavelength which makes a better choice for studies such as optimizing singlet oxygen generation and detection under specific experimental conditions.

Finally, we note that, as with other reactive oxygen species, antioxidants can quench $^1O_2$. This is used, for example, as a protective mechanism against oxidative damage in plants [44]. In mammalian cells, Soares et al. [45] have reported that the local oxidative stress produced by $^1O_2$ during PDT can be mitigated through three main antioxidant mechanisms, namely superoxide dismutase, catalase and glutathione, and that the magnitude of this protective effect is cell type-dependent because of different endogenous levels of these reactants. An important translational issue is whether the "therapeutic window" for PDT damage to tumor versus normal tissues is impacted by their having different concentrations of antioxidants or could be enhanced by the tissue-specific administration of antioxidants. Direct $^1O_2$ luminescence, as presented here, provides an excellent tool for studying these antioxidant effects directly and quantitatively without the potentially confounding use of secondary fluorescent reporters such as $^1O_2$ sensor green.

4. Conclusions

The above results showed that the singlet oxygen ($^1O_2$) lifetime in PpIX photosensitizer is solvent- and microenvironment-dependent, ranging from ~14, ~49, ~29 and ~29 μs in ethanol, acetone, BSA and solid agarose, respectively. Acetone generally exhibits fewer non-radiative decay pathways for singlet oxygen in comparison to ethanol and biological media. This is attributed to the absence of hydrogen bonding, thereby leading to an extended lifetime [46–48]. The longer lifetime of $^1O_2$ in BSA and agarose phantom, compared to ethanol, can be attributed to a combination of factors, including quenching interactions facilitated by protective protein interactions, viscosity, restricted diffusion due to the presence of hydrophilic and hydrophobic grooves, and physical properties (air-filled porosity, bulk density, shrinkage, etc.) of the biological media [49–51]. The singlet oxygen is highly reactive and short-lived; therefore, a small variation in $^1O_2$ lifetime alters its reactivity and diffusivity. Esben Skovsen et al. (2005) demonstrated that singlet oxygen can have a surprisingly long lifetime within cells, allowing it to diffuse over considerable distances [52]. Also, a shorter lifetime of triplet-state photosensitizers such as 0.16 μs has been reported in BSA compared to agarose or ethanol due to quenching interactions with the protein and the complex microenvironment within BSA [51,53].

In the context of Intralipid studies, it has been observed that the binding of PpIX to lipoproteins has the potential to modify the lifetime of singlet oxygen. This modification arises from the possible quenching of singlet oxygen by lipoproteins [40]. The phenomenon of increased scattering can lead to a prolonged residence time of the triplet state in the excited state. Consequently, this can result in diminished energy transfer efficiency and an extension of the triplet lifetime [41]. Overall, the effects on the measurement are altered due to light scattering and possible binding/interactions of the PpIX with the Intralipid lipoproteins.

The TSOLD system used in this study is a significant advance over earlier instruments [16,17], featuring a nanosecond pulsed diode laser with a tunable pulse width and pulse rate capabilities. Notably, this system is considerably more compact and lower-cost than its predecessors [19,29]. The system's performance was confirmed through the detection of the $^1O_2$ signal from PpIX in ethanol, where the 1270 nm counts were significantly higher relative to the background than published values [19]. In the next stage of system

engineering, the bifurcated fiber bundle coupled with an ns pulsed laser will further reduce the footprint of the system, further improving its practicality, especially for in vivo and clinical use.

In summary, the measurement of the PpIX concentration dependence of the luminescence generation in different solvents and biological media demonstrated that the $^1O_2$ generation and lifetime are affected by changes in microenvironmental factors. Optical scattering in biological tissues also affects the spatial distribution of excitation light, and thereby of the $^1O_2$ generation, as well as the near-infrared luminescence [54,55]. Also, quenching and diffusion limitations in biological media further reduce the $^1O_2$ lifetime [54]. Hence, these multiple factors need to be taken into account during $^1O_2$ luminescence measurements for PDT dosimetry, especially where absolute singlet oxygen concentrations are used to predict or correlate with the biological outcomes of the treatment. In addition, the singlet oxygen lifetime directly affects the effective diffusion range at cellular/subcellular scales [51], and previous studies have shown that, because of the very short $^1O_2$ lifetime, the localization of the photosensitizer in different organelles has a marked impact on the cytotoxicity even for the same concentration of singlet oxygen [56].

Author Contributions: Conceptualization, V.V., B.C.W., T.C.Z. and R.H.H.; methodology, V.V., B.C.W., T.C.Z. and R.H.H.; software, V.V. and R.H.H.; validation, V.V. and R.H.H.; formal analysis, V.V., B.C.W. and R.H.H.; investigation, V.V. and R.H.H.; resources, V.V. and R.H.H.; data curation, V.V.; writing—original draft preparation, V.V.; writing—review and editing, V.V., W.Y., B.C.W., T.C.Z. and R.H.H.; visualization, V.V., B.C.W., T.C.Z. and R.H.H.; supervision, B.C.W., T.C.Z. and R.H.H.; project administration, T.C.Z. and R.H.H.; funding acquisition, T.C.Z. and R.H.H. All authors have read and agreed to the published version of the manuscript.

Institutional Review Board Statement: Not applicable.

Informed Consent Statement: Not applicable.

Data Availability Statement: The raw data supporting the conclusions of this article will be made available by the authors on request.

Conflicts of Interest: The authors declare no conflicts of interest.

References

1. Brown, S.B.; Brown, E.A.; Walker, I. The Present and Future Role of Photodynamic Therapy in Cancer Treatment. *Lancet Oncol.* **2004**, *5*, 497–508. [CrossRef] [PubMed]
2. Agostinis, P.; Berg, K.; Cengel, K.A.; Foster, T.H.; Girotti, A.W.; Gollnick, S.O.; Hahn, S.M.; Hamblin, M.R.; Juzeniene, A.; Kessel, D.; et al. Photodynamic Therapy of Cancer: An Update. *CA A Cancer J. Clin.* **2011**, *61*, 250–281. [CrossRef] [PubMed]
3. Dolmans, D.E.J.G.J.; Fukumura, D.; Jain, R.K. Photodynamic Therapy for Cancer. *Nat. Rev. Cancer* **2003**, *3*, 380–387. [CrossRef]
4. Wilson, B.C.; Patterson, M.S.; Lilge, L. Implicit and Explicit Dosimetry in Photodynamic Therapy: A New Paradigm. *Laser Med. Sci.* **1997**, *12*, 182–199. [CrossRef]
5. Bankó, C.; Nagy, Z.L.; Nagy, M.; Szemán-Nagy, G.G.; Rebenku, I.; Imre, L.; Tiba, A.; Hajdu, A.; Szöllősi, J.; Kéki, S.; et al. Isocyanide Substitution in Acridine Orange Shifts DNA Damage-Mediated Phototoxicity to Permeabilization of the Lysosomal Membrane in Cancer Cells. *Cancers* **2021**, *13*, 5652. [CrossRef]
6. Castano, A.P.; Demidova, T.N.; Hamblin, M.R. Mechanisms in Photodynamic Therapy: Part One—Photosensitizers, Photochemistry and Cellular Localization. *Photodiagnosis Photodyn. Ther.* **2004**, *1*, 279–293. [CrossRef]
7. Gunaydin, G.; Gedik, M.E.; Ayan, S. Photodynamic Therapy—Current Limitations and Novel Approaches. *Front. Chem.* **2021**, *9*, 691697. [CrossRef]
8. Plaetzer, K.; Krammer, B.; Berlanda, J.; Berr, F.; Kiesslich, T. Photophysics and Photochemistry of Photodynamic Therapy: Fundamental Aspects. *Lasers Med. Sci.* **2009**, *24*, 259–268. [CrossRef]
9. Montaseri, H.; Kruger, C.A.; Abrahamse, H. Review: Organic Nanoparticle Based Active Targeting for Photodynamic Therapy Treatment of Breast Cancer Cells. *Oncotarget* **2020**, *11*, 2120–2136. [CrossRef]

10. Kim, M.; Penjweini, R.; Gemmell, N.; Veilleux, I.; McCarthy, A.; Buller, G.; Hadfield, R.; Wilson, B.; Zhu, T. A Comparison of Singlet Oxygen Explicit Dosimetry (SOED) and Singlet Oxygen Luminescence Dosimetry (SOLD) for Photofrin-Mediated Photodynamic Therapy. *Cancers* **2016**, *8*, 109. [CrossRef]

11. Kim, M.M.; Darafsheh, A. Light Sources and Dosimetry Techniques for Photodynamic Therapy. *Photochem. Photobiol.* **2020**, *96*, 280–294. [CrossRef] [PubMed]

12. Niedre, M.; Patterson, M.S.; Wilson, B.C. Direct Near-Infrared Luminescence Detection of Singlet Oxygen Generated by Photodynamic Therapy in Cells In Vitro and Tissues In Vivo. *Photochem. Photobiol.* **2002**, *75*, 382–391. [CrossRef] [PubMed]

13. Jarvi, M.T.; Niedre, M.J.; Patterson, M.S.; Wilson, B.C. Singlet Oxygen Luminescence Dosimetry (SOLD) for Photodynamic Therapy: Current Status, Challenges and Future Prospects. *Photochem. Photobiol.* **2006**, *82*, 1198–1210. [CrossRef] [PubMed]

14. Hackbarth, S.; Islam, W.; Fang, J.; Subr, V.; Röder, B.; Etrych, T.; Maeda, H. Singlet Oxygen Phosphorescence Detection in Vivo Identifies PDT-Induced Anoxia in Solid Tumors. *Photochem. Photobiol. Sci.* **2019**, *18*, 1304–1314. [CrossRef] [PubMed]

15. Kim, I.-W.; Park, J.M.; Roh, Y.J.; Kim, J.H.; Choi, M.-G.; Hasan, T. Direct Measurement of Singlet Oxygen by Using a Photomultiplier Tube-Based Detection System. *J. Photochem. Photobiol. B Biol.* **2016**, *159*, 14–23. [CrossRef]

16. Boso, G.; Ke, D.; Korzh, B.; Bouilloux, J.; Lange, N.; Zbinden, H. Time-Resolved Singlet-Oxygen Luminescence Detection with an Efficient and Practical Semiconductor Single-Photon Detector. *Biomed. Opt. Express* **2016**, *7*, 211. [CrossRef]

17. Gemmell, N.R.; McCarthy, A.; Liu, B.; Tanner, M.G.; Dorenbos, S.D.; Zwiller, V.; Patterson, M.S.; Buller, G.S.; Wilson, B.C.; Hadfield, R.H. Singlet Oxygen Luminescence Detection with a Fiber-Coupled Superconducting Nanowire Single-Photon Detector. *Opt. Express* **2013**, *21*, 5005. [CrossRef]

18. Hadfield, R.H.; Leach, J.; Fleming, F.; Paul, D.J.; Tan, C.H.; Ng, J.S.; Henderson, R.K.; Buller, G.S. Single-Photon Detection for Long-Range Imaging and Sensing. *Optica* **2023**, *10*, 1124. [CrossRef]

19. Gemmell, N.R.; McCarthy, A.; Kim, M.M.; Veilleux, I.; Zhu, T.C.; Buller, G.S.; Wilson, B.C.; Hadfield, R.H. A Compact Fiber-optic Probe-based Singlet Oxygen Luminescence Detection System. *J. Biophotonics* **2017**, *10*, 320–326. [CrossRef]

20. Morozov, P.; Lukina, M.; Shirmanova, M.; Divochiy, A.; Dudenkova, V.; Gol'tsman, G.N.; Becker, W.; Shcheslavskiy, V.I. Singlet Oxygen Phosphorescence Imaging by Superconducting Single-Photon Detector and Time-Correlated Single-Photon Counting. *Opt. Lett.* **2021**, *46*, 1217. [CrossRef]

21. Hackbarth, S.; Pfitzner, M.; Pohl, J.; Röder, B. Time-Resolved Singlet Oxygen Luminescence Ex Vivo. In *Singlet Oxygen Detection and Imaging*; Synthesis Lectures on Materials and Optics; Springer International Publishing: Cham, Switzerland, 2021; pp. 61–80. ISBN 978-3-031-01263-1.

22. Niedre, M.J.; Patterson, M.S.; Giles, A.; Wilson, B.C. Imaging of Photodynamically Generated Singlet Oxygen Luminescence In Vivo. *Photochem. Photobiol.* **2005**, *81*, 941–943. [CrossRef] [PubMed]

23. Sarbadhikary, P.; George, B.P.; Abrahamse, H. Recent Advances in Photosensitizers as Multifunctional Theranostic Agents for Imaging-Guided Photodynamic Therapy of Cancer. *Theranostics* **2021**, *11*, 9054–9088. [CrossRef] [PubMed]

24. Sun, H.; Guo, R.; Guo, Y.; Song, J.; Li, Z.; Song, F. Boosting Type-I and Type-II ROS Production of Water-Soluble Porphyrin for Efficient Hypoxic Tumor Therapy. *Mol. Pharm.* **2023**, *20*, 606–615. [CrossRef]

25. Yan, T.; Alimu, G.; Zhu, L.; Fan, H.; Zhang, L.; Du, Z.; Ma, R.; Chen, S.; Alifu, N.; Zhang, X. PpIX/IR-820 Dual-Modal Therapeutic Agents for Enhanced PDT/PTT Synergistic Therapy in Cervical Cancer. *ACS Omega* **2022**, *7*, 44643–44656. [CrossRef]

26. Myrzakhmetov, B.; Arnoux, P.; Mordon, S.; Acherar, S.; Tsoy, I.; Frochot, C. Photophysical Properties of Protoporphyrin IX, Pyropheophorbide-a, and Photofrin® in Different Conditions. *Pharmaceuticals* **2021**, *14*, 138. [CrossRef]

27. Vikas, V.; Kumar, R.; Soni, S. Dynamic Change in Optical Properties of a Nanoparticle Embedded Tumor Phantom for Plasmonic Photothermal Cancer Therapeutics. *J. Biophotonics* **2023**, *16*, e202200179. [CrossRef]

28. Protoporphyrin IX = 95 553-12-8. Available online: http://www.sigmaaldrich.com/ (accessed on 6 May 2024).

29. Tsimvrakidis, K.; Gemmell, N.R.; Erotokritou, K.; Miki, S.; Yabuno, M.; Yamashita, T.; Terai, H.; Hadfield, R.H. Enhanced Optics for Time-Resolved Singlet Oxygen Luminescence Detection. *IEEE J. Select. Top. Quantum Electron.* **2019**, *25*, 7000107. [CrossRef]

30. Jones, L.R.; Grossweiner, L.I. Singlet Oxygen Generation by Photofrin® in Homogeneous and Light-Scattering Media. *J. Photochem. Photobiol. B Biol.* **1994**, *26*, 249–256. [CrossRef]

31. Flock, S.T.; Jacques, S.L.; Wilson, B.C.; Star, W.M.; van Gemert, M.J.C. Optical Properties of Intralipid: A Phantom Medium for Light Propagation Studies. *Lasers Surg. Med.* **1992**, *12*, 510–519. [CrossRef]

32. Krasnovsky, A.A. Singlet Molecular Oxygen in Photobiochemical Systems: IR Phosphorescence Studies. *Membr. Cell Biol.* **1998**, *12*, 665–690.

33. Vinklárek, I.S.; Scholz, M.; Dědic, R.; Hála, J. Singlet Oxygen Feedback Delayed Fluorescence of Protoporphyrin IX in Organic Solutions. *Photochem. Photobiol. Sci.* **2017**, *16*, 507–518. [CrossRef] [PubMed]

34. Aebisher, D.; Serafin, I.; Batóg-Szczęch, K.; Dynarowicz, K.; Chodurek, E.; Kawczyk-Krupka, A.; Bartusik-Aebisher, D. Photodynamic Therapy in the Treatment of Cancer—The Selection of Synthetic Photosensitizers. *Pharmaceuticals* **2024**, *17*, 932. [CrossRef] [PubMed]

35. DeRosa, M. Photosensitized Singlet Oxygen and Its Applications. *Coord. Chem. Rev.* **2002**, *233–234*, 351–371. [CrossRef]

36.   Ricchelli, F. Photophysical Properties of Porphyrins in Biological Membranes. *J. Photochem. Photobiol. B Biol.* **1995**, *29*, 109–118. [CrossRef] [PubMed]

37.   Ogilby, P.R. Singlet Oxygen: There Is Indeed Something New under the Sun. *Chem. Soc. Rev.* **2010**, *39*, 3181. [CrossRef]

38.   Hu, Y.; Lin, L.; Liu, L.; Yu, Y.; Liao, X.; Gu, Y.; Li, B. Detection of Singlet Oxygen Luminescence in Skin Phantom Based on Optical Fiber Detection. In Proceedings of the Optics in Health Care and Biomedical Optics IX; Luo, Q., Li, X., Tang, Y., Gu, Y., Zhu, D., Eds.; SPIE: Hangzhou, China, 2019; p. 106.

39.   Sitte, E.; Senge, M.O. The Red Color of Life Transformed—Synthetic Advances and Emerging Applications of Protoporphyrin IX in Chemical Biology. *Eur. J. Org. Chem.* **2020**, *2020*, 3171–3191. [CrossRef]

40.   Yeh, P.-S.; Li, C.-C.; Lu, Y.-S.; Chiang, Y.-W. Structural Insights into the Binding and Degradation Mechanisms of Protoporphyrin IX by the Translocator Protein TSPO. *JACS Au* **2023**, *3*, 2918–2929. [CrossRef]

41.   Hussain, M.; Razi, S.S.; Tao, T.; Hartl, F. Triplet-Triplet Annihilation Photon up-Conversion: Accessing Triplet Excited States with Minimum Energy Loss. *J. Photochem. Photobiol. C Photochem. Rev.* **2023**, *56*, 100618. [CrossRef]

42.   Solubility of Softisan 100 in Ethanol + Water and Acetone + Water Solutions. *J. Chem. Eng. Data* **2010**, *55*, 2333–2337. [CrossRef]

43.   Sakamoto, K.; Ohno-Okumura, E. Syntheses and Functional Properties of Phthalocyanines. *Materials* **2009**, *2*, 1127–1179. [CrossRef]

44.   Tournaire, C.; Croux, S.; Maurette, M.-T.; Beck, I.; Hocquaux, M.; Braun, A.M.; Oliveros, E. Antioxidant Activity of Flavonoids: Efficiency of Singlet Oxygen (1Δg) Quenching. *J. Photochem. Photobiol. B Biol.* **1993**, *19*, 205–215. [CrossRef] [PubMed]

45.   Soares, H.T.; Campos, J.R.S.; Gomes-da-Silva, L.C.; Schaberle, F.A.; Dabrowski, J.M.; Arnaut, L.G. Pro-Oxidant and Antioxidant Effects in Photodynamic Therapy: Cells Recognise That Not All Exogenous ROS Are Alike. *Chembiochem* **2016**, *17*, 836–842. [CrossRef] [PubMed]

46.   Figueiredo, T.L.C.; Johnstone, R.A.W.; Sørensen, A.M.P.S.; Burget, D.; Jacques, P. Determination of Fluorescence Yields, Singlet Lifetimes and Singlet Oxygen Yields of Water-Insoluble Porphyrins and Metalloporphyrins in Organic Solvents and in Aqueous Media. *Photochem. Photobiol.* **1999**, *69*, 517–528. [CrossRef]

47.   Wilkinson, F.; Helman, W.P.; Ross, A.B. Quantum Yields for the Photosensitized Formation of the Lowest Electronically Excited Singlet State of Molecular Oxygen in Solution. *J. Phys. Chem. Ref. Data* **1993**, *22*, 113–262. [CrossRef]

48.   Mano, C.M.; Prado, F.M.; Massari, J.; Ronsein, G.E.; Martinez, G.R.; Miyamoto, S.; Cadet, J.; Sies, H.; Medeiros, M.H.G.; Bechara, E.J.H.; et al. Excited Singlet Molecular O2 (1Δg) Is Generated Enzymatically from Excited Carbonyls in the Dark. *Sci. Rep.* **2014**, *4*, 5938. [CrossRef]

49.   Giménez, R.E.; Vargová, V.; Rey, V.; Turbay, M.B.E.; Abatedaga, I.; Morán Vieyra, F.E.; Paz Zanini, V.I.; Mecchia Ortiz, J.H.; Katz, N.E.; Ostatná, V.; et al. Interaction of Singlet Oxygen with Bovine Serum Albumin and the Role of the Protein Nano-Compartmentalization. *Free Radic. Biol. Med.* **2016**, *94*, 99–109. [CrossRef]

50.   Miranda-Apodaca, J.; Hananya, N.; Velázquez-Campoy, A.; Shabat, D.; Arellano, J.B. Emissive Enhancement of the Singlet Oxygen Chemiluminescence Probe after Binding to Bovine Serum Albumin. *Molecules* **2019**, *24*, 2422. [CrossRef]

51.   Kuimova, M.K.; Yahioglu, G.; Ogilby, P.R. Singlet Oxygen in a Cell: Spatially Dependent Lifetimes and Quenching Rate Constants. *J. Am. Chem. Soc.* **2009**, *131*, 332–340. [CrossRef]

52.   Skovsen, E.; Snyder, J.W.; Lambert, J.D.C.; Ogilby, P.R. Lifetime and Diffusion of Singlet Oxygen in a Cell. *J. Phys. Chem. B* **2005**, *109*, 8570–8573. [CrossRef]

53.   Takemura, T.; Ohta, N.; Nakajima, S.; Sakata, I. Critical Importance of the Triplet Lifetime of Photosensitizer in Photodynamic Therapy of Tumor. *Photochem. Photobiol.* **1989**, *50*, 339–344. [CrossRef]

54.   Codognato, D.C.K.; Pena, F.S.; dos Reis, E.R.; Ramos, A.P.; Borissevitch, I.E. Effects of Serum Albumin on the Photophysical Characteristics of Synthetic and Endogenous Protoporphyrin IX. *Braz. J. Med. Biol. Res.* **2022**, *55*, e12272. [CrossRef] [PubMed]

55.   Reinert, M.; Piffaretti, D.; Wilzbach, M.; Hauger, C.; Guckler, R.; Marchi, F.; D'Angelo, M.L. Quantitative Modulation of PpIX Fluorescence and Improved Glioma Visualization. *Front. Surg.* **2019**, *6*, 41. [CrossRef] [PubMed]

56.   Weston, M.A.; Patterson, M.S. Chapter 33. Singlet Oxygen Dosimetry in Biological Media. In *Comprehensive Series in Photochemical & Photobiological Sciences*; Nonell, S., Flors, C., Eds.; Royal Society of Chemistry: Cambridge, UK, 2016; Volume 2, pp. 151–168, ISBN 978-1-78262-697-8.